nature nanotechnology

LETTERS

https://doi.org/10.1038/s41565-018-0084-4

Kinesin expands and stabilizes the GDP-microtubule lattice

Daniel R. Peet[1,2], Nigel J. Burroughs[2,3] and Robert A. Cross[1*]

Kinesin-1 is a nanoscale molecular motor that walks towards the fast-growing (plus) ends of microtubules, hauling molecular cargo to specific reaction sites in cells. Kinesin-driven transport is central to the self-organization of eukaryotic cells and shows great promise as a tool for nano-engineering[1]. Recent work hints that kinesin may also play a role in modulating the stability of its microtubule track, both in vitro[2,3] and in vivo[4], but the results are conflicting[5–7] and the mechanisms are unclear. Here, we report a new dimension to the kinesin–microtubule interaction, whereby strong-binding state (adenosine triphosphate (ATP)-bound and apo) kinesin-1 motor domains inhibit the shrinkage of guanosine diphosphate (GDP) microtubules by up to two orders of magnitude and expand their lattice spacing by ~1.6%. Our data reveal an unexpected mechanism by which the mechanochemical cycles of kinesin and tubulin interlock, and so allow motile kinesins to influence the structure, stability and mechanics of their microtubule track.

As kinesin molecules walk along microtubules, their motor domains cycle through a series of nucleotide-specific conformations. We tested whether these different nucleotide states of kinesin-1 motor domains influence microtubule stability. First, we attached fluorescent microtubule 'seeds' to the inside of a flow chamber via biotin–NeutrAvidin linkages and flowed in guanosine triphosphate (GTP)–tubulin, which caused dynamic microtubules to grow from the seeds (Fig. 1a). We then initiated microtubule depolymerization by washing out tubulin, while simultaneously flowing in monomeric kinesin-1 motor domains. We initially tested the effect of a kinesin motor-domain mutant (T93N) that enriches the apo state of the motor[8]. The apo state of kinesin is a strong-binding state, which means that it binds tightly and stereospecifically to microtubules[9]. We found that T93N reduced microtubule shrinkage to 1% of the control rate (Fig. 1b,c). We then used wild-type kinesin motor domains supplemented with either adenylyl-imidodiphosphate (AMPPNP), a non-hydrolysable ATP analogue that causes a strong-binding state, or adenosine diphosphate (ADP), which causes a weak-binding state, and compared their effects. Wild-type kinesin is immotile in AMPPNP and ADP. We found that AMPPNP–wild-type kinesin inhibited microtubule shrinkage similarly to T93N, whereas ADP–wild-type kinesin had no detectable effect (Fig. 1c). We conclude that the strong-binding states of kinesin powerfully inhibit the shrinkage of GDP microtubules.

Next, we bound GDP microtubules to a kinesin-coated coverslip in a flow chamber, triggered depolymerization by washing out the residual GTP–tubulin and again observed microtubule shrinkage (Fig. 2a). Geometric constraints suggest that in this arrangement at most five protofilaments (PFs) can bind to the kinesin surface (Fig. 2b). Despite this, entire microtubules were stabilized (Fig. 2c). We then flowed solutions through the channel in two steps (Fig. 2a). First, ADP was flowed in, which reduced the fraction of kinesins in a strong-binding state and thereby increased the microtubule-shrinkage rate (Fig. 2c and Supplementary Movie 1). By titrating the ADP concentration, we found that microtubule-shrinkage rates could be fine-tuned over two orders of magnitude (Fig. 2d and Supplementary Table 1). Comparing the maximal inhibition of microtubule shrinkage by kinesin in solution (0.21 ± 0.02 (25) dimer PF^{-1} s^{-1} (mean ± s.e.m. (n))) with that of the kinesin surface (0.06 ± 0.01 (6) dimer PF^{-1} s^{-1} in the presence of 400 nM ADP) shows that surface immobilization enhances the stabilizing effect of kinesin, despite kinesin binding being restricted to only a subset of PFs.

Frequently, faint fluorescent trails were visible on the kinesin-coated surface in the wake of retreating microtubule tips. These shrank endwise on the addition of ADP, which suggests that their tubulin is still assembled into PFs (Fig. 2c and Supplementary Movie 1). Trails were tapered, and fluorescence-intensity analysis (Fig. 3a, Supplementary Methods and Supplementary Figs. 1 and 2) indicated that they contain 2–3 PFs at their tips (Fig. 3b). On average, trails can shrink faster than their microtubule stem because they appear transiently, typically forming, lengthening and retracting multiple times during the shrinkage of each surface-attached microtubule (Supplementary Fig. 3). As a final step in these experiments, we flowed in a buffer that contained taxol and ATP, which triggered kinesin-driven sliding to reveal the microtubule polarity.

Why does a kinesin-coated surface stabilize microtubules but also cause them to split? Taxol-stabilized microtubules have recently been shown to split on a kinesin-coated surface[10]. However, ATP-driven kinesin stepping was essential to this process, which is not the case for our taxol-free GDP microtubules. Several strands of evidence suggest that kinesin binding can change the lattice conformation and mechanics of microtubules. A kinesin-coated surface has been reported to reduce the Young's modulus of taxol-stabilized microtubules[11]. Structural changes have also been reported after kinesin binding to taxol-stabilized[12] and guanosine-5′-((α,β)-methyleno)triphosphate (GMPCPP)-bound microtubules[13]. Furthermore, the longitudinal compaction of the microtubule lattice that accompanies GTP hydrolysis is reduced in kinesin-bound microtubules[14], which suggests that kinesin influences the longitudinal spacing between tubulin subunits in the microtubule lattice. We therefore hypothesized that kinesin binding modifies the axial spacing between GDP–tubulin subunits in the microtubule lattice. Binding kinesins to one side of a microtubule, as in our surface assay, would then change the lattice spacing on that side, but not the other, and so cause shear stress that could facilitate splitting.

To test the idea that kinesin binding stabilizes a distinct conformation of the microtubule lattice, we used hydrodynamic flow to

[1]Centre for Mechanochemical Cell Biology, Warwick Medical School, Coventry, UK. [2]Warwick Systems Biology Centre, University of Warwick, Coventry, UK. [3]Mathematics Institute, University of Warwick, Coventry, UK. *e-mail: R.A.Cross@warwick.ac.uk

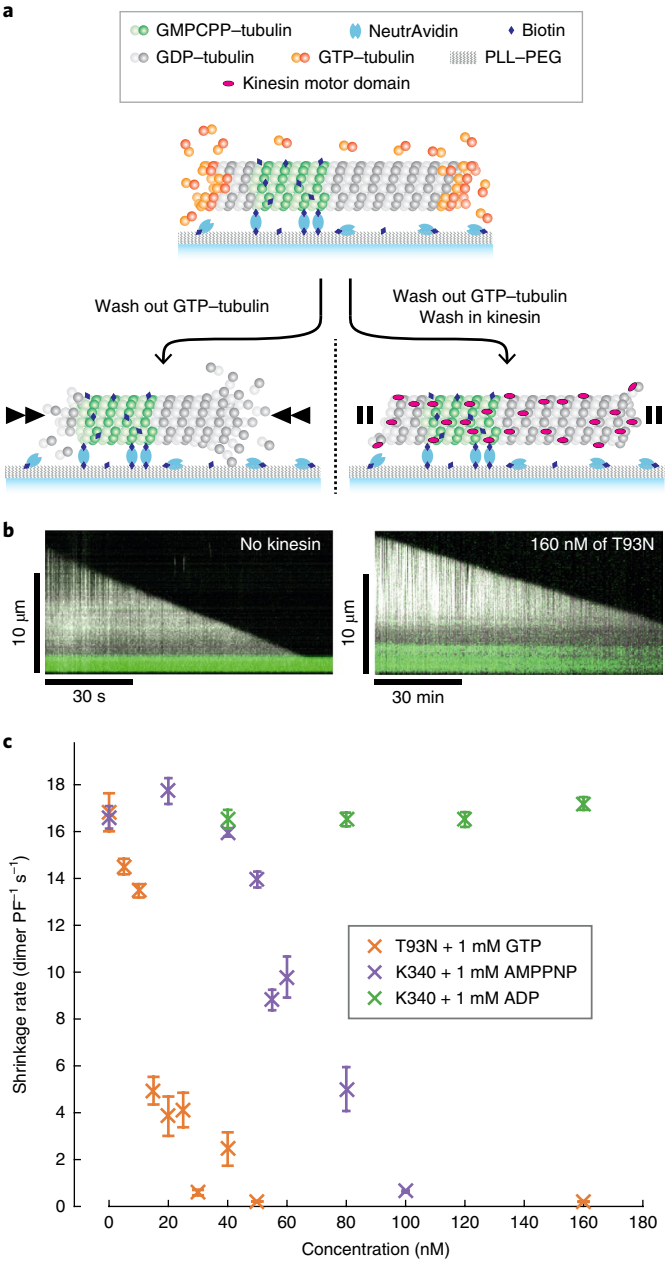

Fig. 1 | Strong-binding-state kinesins inhibit GDP-microtubule shrinkage. **a**, Schematic representation of a tubulin-depletion assay. Dynamic microtubules shrink rapidly when GTP-tubulin is depleted (left) unless bound to strong-binding-state kinesins (right). **b**, Representative kymographs of microtubules that shrink in the absence (left) and presence (right) of T93N (with different timescales). Dynamic microtubules are shown in white (dark field) and fluorescent seeds in green (epifluorescence). **c**, Shrinkage rates of microtubules in the presence of kinesins and nucleotides. GTP was included with T93N only. Error bars are mean ± s.e.m. We analysed a total of $n = 317$, 225 and 168 microtubules for the T93N–GTP, wild-type–AMPPNP and wild-type–ADP conditions, respectively.

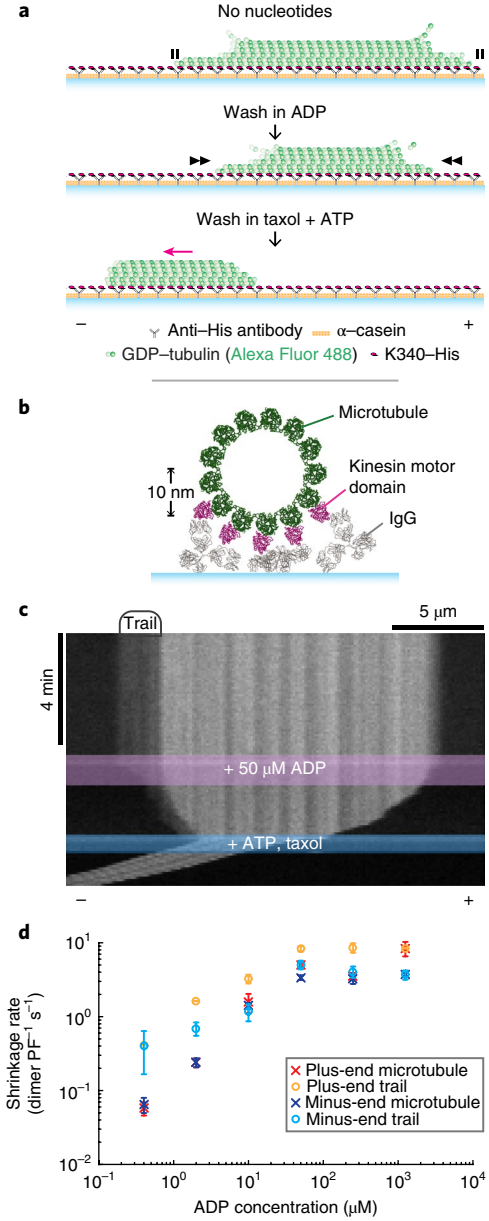

Fig. 2 | Microtubules are stabilized when kinesins bind to one side of the lattice. **a**, Schematic of a kinesin surface-clamp assay. The microtubule polarity is labelled – and +. **b**, Cross-sectional view of a kinesin surface-clamp assay that shows immunoglobulin G (PDB:1IGY) and kinesin-bound microtubule (PDB:4UXT) structures to provide scale. **c**, Representative kymograph of a microtubule in a kinesin surface-clamp. **d**, Average shrinkage rates of microtubules and their trails. Error bars are mean ± s.e.m, which reflects the intermicrotubule variability. The n values are given in Supplementary Table 1.

bend tethered dynamic microtubules, and thereby expand the microtubule lattice on the convex side and compact it on the concave side (Fig. 4 and Supplementary Movie 2). We supplemented T93N into the flow and observed the mechanical response of the microtubules on stopping the flow. In the absence of kinesins, the microtubules quickly recoiled to a straight conformation and rapidly depolymerized. Remarkably, low concentrations of T93N (15–30 nM) blocked this recoil and effectively locked the GDP microtubules in a curved conformation as well as inhibited their shrinkage. These data suggest that, indeed, strong-binding-state kinesins preferentially bind and stabilize a distinct longitudinal lattice spacing of GDP microtubules.

We noticed that in the presence of higher concentrations of kinesin (≥50 nM), the curved microtubules tended to re-straighten slowly. To explain this observation, we speculate that strong-binding-state kinesins bind preferentially, but not exclusively, to one side of the curved microtubules. At high kinesin concentrations, the favoured side of the microtubule would then quickly become

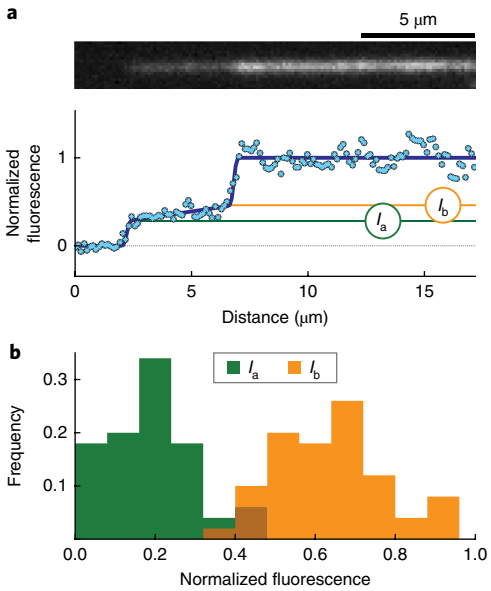

Fig. 3 | Subsets of PFs are stabilized by a kinesin-coated surface. **a**, Model fit to the intensity profile of a microtubule tip (bottom) with the associated fluorescence image (top). I_a is the intensity at the tip and I_b at the base of the trail. **b**, Histogram of I_a and I_b values for microtubules ($n = 50$), normalized to the intensities of their parent microtubules in the no-nucleotide phase of the experiment. Mean ± s.d. values are 0.19 ± 0.11 (2–3 PFs) and 0.64 ± 0.13 (8–9 PFs) for I_a and I_b, respectively.

fully occupied, and binding would continue more slowly on the unfavoured side, which ultimately drives the microtubule back into a straight conformation (Fig. 4b). Kinesins have previously been reported to bind preferentially to GTP microtubules, which have an expanded lattice spacing compared with GDP microtubules[15]. In the light of this, we postulated that strong-binding-state kinesins drive an increase in the lattice spacing of GDP microtubules.

To test this point directly, we grew dynamic microtubules as in the previous experiments, but this time we capped their exposed tips with non-biotinylated fluorescent GMPCPP–tubulin to produce stable GDP microtubules that were tethered to the surface only at one end (Fig. 5a). The GDP-microtubules and their stabilized caps were labelled fluorescently in different colours and imaged using total internal reflection fluorescence (TIRF) microscopy. We used pressure-driven microfluidics to align the microtubules in a constant hydrodynamic flow that contained either wild-type apo-kinesin motor domains or 1 mM ADP. When kinesin was introduced, the GDP-bound segment of the microtubule lengthened as predicted (Fig. 5b and Supplementary Movie 3).

TIRF microscopy visualizes an optical section ~100 nm deep and microtubules remained visible throughout our experiment, which indicates that the flow constrained them within this 100 nm thick section. Strikingly, microtubules briefly crinkled on switching from ADP to kinesin, causing them to dip in and out of the TIRF illumination (Supplementary Movie 4). This transient crinkling can also be seen in our initial microtubule bending experiments (≥50 nM in Supplementary Movie 2). The crinkles progressively straightened (within 10–30 s) to reveal that the microtubule had expanded. Switching to ADP caused microtubules to recoil quickly to their

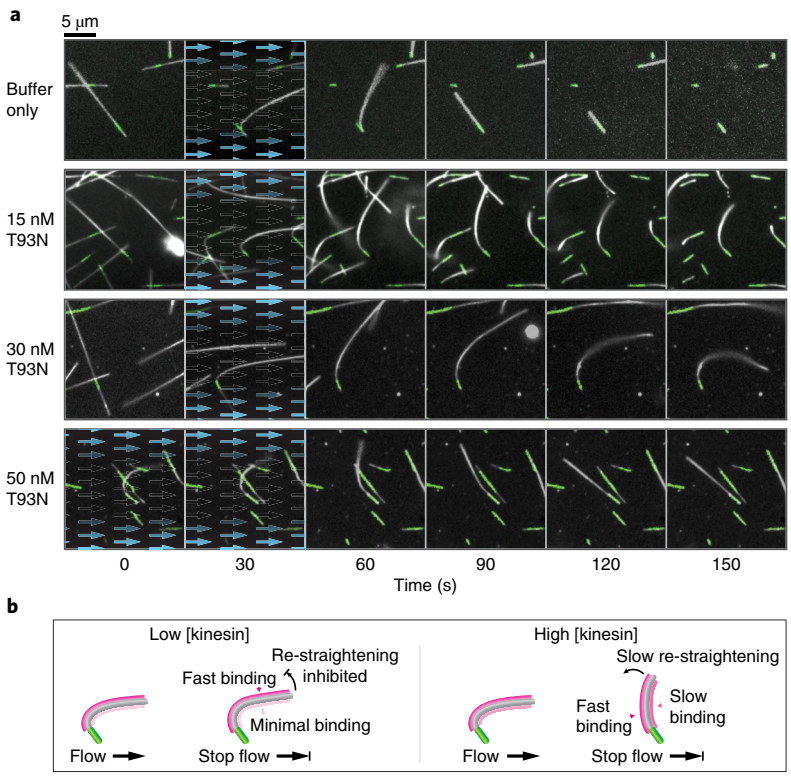

Fig. 4 | Nucleotide-free motor domains can bend-lock microtubules. a, Time-lapse images of microtubule bending experiments for a range of kinesin concentrations. Blue arrows highlight the presence and direction of fluid flow. Dynamic microtubules appear white (dark field) and fluorescent seeds are marked in green (epifluorescence). Each condition was tested twice on independent occasions. The microtubules shown here were selected for their similar orientations. A more extensive selection is given in Supplementary Movie 2, which shows a complete range of orientations and lengths. **b**, Working model. We propose that kinesin binds preferentially to the stretched (convex) side of the microtubule and also stabilizes this expanded region of the microtubule lattice. At high kinesin concentrations, the convex side of the microtubule would quickly saturate. Binding would also occur slowly on the concave side, and so cause this side to expand and progressively re-straighten the microtubule.

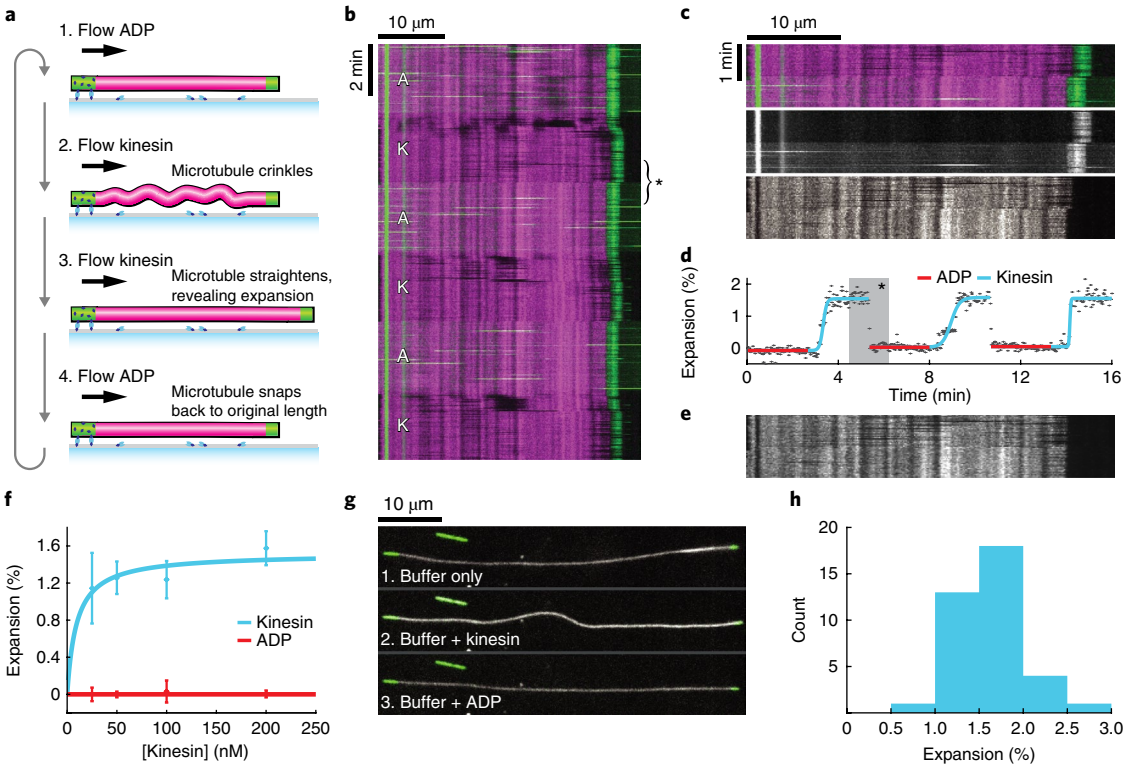

Fig. 5 | Kinesin increases the lattice spacing of GDP microtubules. a, Fluorescently labelled GDP microtubules (rhodamine, magenta) were grown from surface-bound GMPCPP–tubulin seeds (Alexa Fluor 488, green) and then capped with GMPCPP–tubulin. Buffer was flowed through the channel at a constant rate and while switching between ADP and kinesin-containing solutions. Microtubules briefly crinkled when kinesin was added at high concentrations before straightening to reveal they had lengthened. The addition of ADP caused immediate recoil of the microtubules to their original lengths. **b**, Representative kymograph of a microtubule that changed length as the flow switched between 1 mM ADP (A)- and 200 nM kinesin (K)-containing buffers. A constant volumetric flow rate was maintained throughout the experiment (74.3 ± 0.3 μl min^{-1}; mean ± s.d., 480 time points). **c**, Magnified region from **b** (asterisked region) that highlights the compaction observed when switching from kinesin-containing to ADP-containing solutions. Top, merge. Middle, green imaging channel (GMPCPP–tubulin and beads). Buffer exchange is visible due to the high background provided by the fluorescent beads (after ~50 s). The untethered (rightmost) tip retracts in <4 s (two frames) on switching to ADP. Bottom, magenta imaging channel (GDP–tubulin). An abrupt rift can be seen in the fiducial markings on the GDP-microtubule when ADP is added. The effect becomes increasingly pronounced further away from the tethered end, consistent with the microtubule lattice uniformly compacting. **d**, Kinesin-driven expansion of the microtubule shown in **b** (the asterisked area again marks the region in **c**). Each data point corresponds to the inverse scaling factor that best maps the given GDP-microtubule profile (row) to match the average profile when ADP was present. The ADP points serve as an internal control for this measurement technique. Supplementary Fig. 5 gives further detail on this method. **e**, Transformed image from **c**, generated by scaling each profile using the inverse of the fitted values in **d**. Such images were used to check for errors visually. Supplementary Animation 1 gives a full-image transformation. **f**, Microtubule expansion measured over a range of kinesin concentrations. A standard binding curve fitted to the mean values is shown, which saturates at 1.52%. Error bars show s.d. *n* values are listed in Supplementary Table 2. **g**, Sequential images of a complementary experiment in which GDP microtubules (shown in white, dark field) were encouraged into the focal plane using methylcellulose and fluid flow was used only intermittently to exchange solutions. When kinesin was added, the microtubule bowed to accommodate the expansion of its lattice between sparse points that were loosely stitched to the surface. The microtubule straightened and shortened on the addition of ADP. **h**, Expansion of surface-stitched GDP microtubules given by the relative contour lengths of GDP microtubules in the presence and absence of kinesin. Mean ± s.d., 1.64 ± 0.39 ($n = 37$ microtubules).

original length (<4 s, two frames in our data) as the kinesin unbound (Fig. 5c,d). Quantification reveals that apo-kinesin binding to the GDP microtubules increases their length by uniformly expanding the microtubule lattice along its axis (Fig. 5c–e and Supplementary Animation 1). The kinesin-induced lattice expansion appears to be fully reversible and the expand-and-recoil cycle can be repeated multiple times (Fig. 5d). We measured the extent of lattice expansion over a range of kinesin concentrations. The increase in lattice spacing saturated at 1.5% (Fig. 5f and Supplementary Table 2).

Occasional point interactions between the microtubules and the surface occurred during these experiments, but these interactions were typically transient and the microtubules visibly quivered in the flow (Supplementary Movies 3 and 4). Under these conditions, kinesin is prohibited from stepping by the absence of ATP and GTP in the imaging buffers. We can therefore rule out the possibility that kinesin generates forces by stepping along the microtubule. As any bending or crinkling produced by kinesin binding will reduce the apparent length of a microtubule in a kymograph, it is possible that our measurements slightly underestimate the full extent of kinesin-induced lattice expansion.

We additionally performed experiments in which we used methylcellulose rather than flow to encourage the microtubules to remain in focus, introducing a flow only intermittently to exchange buffers. Under these conditions, microtubules tended to become 'stitched' to the coverslip at sparse interaction sites. Introducing apo-kinesin then caused the microtubules to bow locally between these tethering points (Fig. 5g and Supplementary Movie 5), which emphasizes the expansion of the lattice. We used 200 nM of apo-kinesin in these experiments, a concentration sufficient to maximize the lattice-expansion effect of kinesin binding (Fig. 5f).

By measuring the change in contour length between the two stabilized microtubule caps, we confirmed that the bowing of the microtubule between tethering points accommodates a 1.6% expansion of the GDP-microtubule lattice (Fig. 5h). Microtubules became more densely 'stitched' to the surface if multiple cycles were performed, but this did not influence the measured expansion (Supplementary Fig. 4). When ADP was flowed through the channel, the microtubules again recoiled to their original lengths (Fig. 5g).

Our data show that strong-binding-state kinesin stabilizes the GDP lattice of dynamic microtubules, and concomitantly increases their axial lattice spacing by 1.6%. Kinesins are known to bind to the intradimer interface of αβ-tubulin, away from the interdimer contacts of the microtubule lattice[13,14,16]. This suggests to us that kinesin binding allosterically modifies the conformation of GDP–tubulin to give it properties more similar to those of GTP–tubulin. Assuming that no twisting of the microtubule occurs, a 1.6% axial expansion equates to approximately 1.3 Å per tubulin dimer (~80 Å), similar to the 1.7 Å difference observed by cryogenic electron microscopy between GMPCPP–microtubule–kinesin and GDP–microtubule–kinesin structures[16]. The strong binding of kinesin has previously been reported to alter the structure of both taxol–GDP microtubules[12] and GMPCPP microtubules[13]. Moreover, a long-range, ATP-dependent cooperative effect has been described whereby the first few kinesins that bind facilitate subsequent binding events in the same region of the microtubule, again suggestive of a kinesin-induced conformational change[17].

We envisage that the ability of strong-binding-state kinesin to stabilize GDP microtubules by inducing a conformational change in their tubulin subunits provides at least a partial mechanistic explanation for the surface-bound depolymerization trails and the bend-locking phenomenon reported here. A microtubule landing on and binding to a kinesin-coated surface would probably become stretched on its surface-bound side. This stretching would create shear stress in the lattice and potentially contribute towards splitting the microtubule to form the trails observed in our kinesin surface-clamp experiments. Similarly, for the microtubule bend locking, expansion of the axial microtubule lattice spacing by 1.6% exclusively on one side of the microtubule would be more than sufficient to account for the observed kinesin stabilization of the curvature. Indeed, full occupancy on one side with zero occupancy on the other would produce a radius of curvature of 1.6 µm, assuming a microtubule has a diameter of 25 nm, far tighter than we observe in any of our post-flow data.

We have worked with kinesin-1, the best-studied kinesin, but it is possible that the mechanism we report here is common to other kinesins. Kif14 is a slow kinesin that binds to microtubules in a rigor-like conformation and inhibits their shrinkage[18]. Kinesin-5 is reported to stabilize PF assemblies during microtubule growth[19], potentially because its strong-binding state stabilizes the polymer. Kip2 also dwells at microtubule ends and increases the microtubule stability[20].

Our work reveals a specific action of strong-binding-state kinesins in stabilizing the GDP lattice of dynamic microtubules. Microtubule-activated ADP release creates a strong (apo) state and this process is affected by the tubulin and kinesin species[21], by post-translational modifications[22] and by the nucleotide state[23] of the microtubule. Importantly, the residence time of kinesin in the strong-binding states is also influenced by mechanical force[24]. Such forces will arise in vivo wherever kinesins do mechanical work, for example, at kinetochores, in microtubule bundles[25], at cortical attachment sites[26] and during the transport of vesicles against a resistance[27]. It is now important to understand the role of these various effects in determining how kinesin motility may feed back on microtubule dynamics.

In conclusion, our data reveal a novel mechanism that allows kinesin-1 to feed back on the structure and stability of its microtubule track. Recent advances in the remote control of kinesin motility, such as photoswitchable fuels[28], suggest the potential for the precise spatial control of these effects.

Methods

Methods, including statements of data availability and any associated accession codes and references, are available at https://doi.org/10.1038/s41565-018-0084-4.

Received: 10 February 2016; Accepted: 30 January 2018;
Published online: 12 March 2018

References

1. Bachand, G. D., Spoerke, E. D. & Stevens, M. J. Microtubule-based nanomaterials: Exploiting nature's dynamic biopolymers. *Biotechnol. Bioeng.* **112**, 1065–1073 (2015).
2. Katsuki, M., Drummond, D. R. & Cross, R. A. Ectopic A-lattice seams destabilize microtubules. *Nat. Commun.* **5**, 3094 (2014).
3. Lombillo, V. A., Stewart, R. J. & McIntosh, J. R. Minus-end-directed motion of kinesin-coated microspheres driven by microtubule depolymerization. *Nature* **373**, 161–164 (1995).
4. Marceiller, J., Drechou, A., Durand, G., Perez, F. & Poüs, C. Kinesin is involved in protecting nascent microtubules from disassembly after recovery from nocodazole treatment. *Exp. Cell. Res.* **304**, 483–492 (2005).
5. Kowalski, R. J. & Williams, R. C. Unambiguous classification of microtubule-ends in vitro: dynamic properties of the plus- and minus-ends. *Cell. Motil. Cytoskelet.* **26**, 282–290 (1993).
6. Daire, V. et al. Kinesin-1 regulates microtubule dynamics via a c-Jun N-terminal kinase-dependent mechanism. *J. Biol. Chem.* **284**, 31992–32001 (2009).
7. Fukata, K. A., Watanabe, H., Iwamatsu, A. & Kaibuchi, K. Tubulin and CRMP-2 complex is transported via kinesin-1. *J. Neurochem.* **93**, 1371–1382 (2005).
8. Nakata, T. & Hirokawa, N. Point mutation of adenosine triphosphate-binding motif generated rigor kinesin that selectively blocks anterograde lysosome membrane transport. *J. Cell. Biol.* **131**, 1039–1053 (1995).
9. Cross, R. A. The kinetic mechanism of kinesin. *Trends Biochem. Sci.* **29**, 301–309 (2004).
10. VanDelinder, V., Adams, P. G. & Bachand, G. D. Mechanical splitting of microtubules into protofilament bundles by surface-bound kinesin-1. *Sci. Rep.* **6**, 39408 (2016).
11. Kabir, A. M. R. et al. Biomolecular motor modulates mechanical property of microtubule. *Biomacromolecules* **15**, 1797–1805 (2014).
12. Krebs, A., Goldie, K. N. & Hoenger, A. Complex formation with kinesin motor domains affects the structure of microtubules. *J. Mol. Biol.* **335**, 139–153 (2004).
13. Morikawa, M. et al. X-ray and cryo-EM structures reveal mutual conformational changes of kinesin and GTP-state microtubules upon binding. *EMBO J.* **34**, 1270–1286 (2015).
14. Alushin, G. M. et al. High-resolution microtubule structures reveal the structural transitions in αβ-tubulin upon GTP hydrolysis. *Cell* **157**, 1117–1129 (2014).
15. Nakata, T., Niwa, S., Okada, Y., Perez, F. & Hirokawa, N. Preferential binding of a kinesin-1 motor to GTP-tubulin-rich microtubules underlies polarized vesicle transport. *J. Cell. Biol.* **194**, 245–255 (2011).
16. Zhang, R., Alushin, G. M., Brown, A. & Nogales, E. Mechanistic origin of microtubule dynamic instability and its modulation by EB proteins. *Cell* **162**, 1–11 (2015).
17. Muto, E. E., Sakai, H. H. & Kaseda, K. K. Long-range cooperative binding of kinesin to a microtubule in the presence of ATP. *J. Cell. Biol.* **168**, 691–696 (2005).
18. Arora, K. et al. KIF14 binds tightly to microtubules and adopts a rigor-like conformation. *J. Mol. Biol.* **426**, 2997–3015 (2014).
19. Chen, Y. & Hancock, W. O. Kinesin-5 is a microtubule polymerase. *Nat. Commun.* **6**, 8160 (2015).
20. Hibbel, A. et al. Kinesin Kip2 enhances microtubule growth in vitro through length-dependent feedback on polymerization and catastrophe. *eLife* **4**, e10542 (2015).
21. Alonso, M. C. et al. An ATP gate controls tubulin binding by the tethered head of kinesin-1. *Science* **316**, 120–123 (2007).
22. Sirajuddin, M., Rice, L. M. & Vale, R. D. Regulation of microtubule motors by tubulin isotypes and post-translational modifications. *Nat. Cell. Biol.* **16**, 335–344 (2014).
23. Vale, R. D., Coppin, C. M., Malik, F., Kull, F. J. & Milligan, R. A. Tubulin GTP hydrolysis influences the structure, mechanical properties, and kinesin-driven transport of microtubules. *J. Biol. Chem.* **269**, 23769–23775 (1994).

24. Carter, N. J. & Cross, R. A. Mechanics of the kinesin step. *Nature* **435**, 308–312 (2005).
25. Cross, R. A. & McAinsh, A. Prime movers: the mechanochemistry of mitotic kinesins. *Nat. Rev. Mol. Cell. Biol.* **15**, 257–271 (2014).
26. Hendricks, A. G. et al. Dynein tethers and stabilizes dynamic microtubule plus ends. *Curr. Biol.* **22**, 632–637 (2012).
27. Blehm, B. H., Schroer, T. A., Trybus, K. M., Chemla, Y. R. & Selvin, P. R. In vivo optical trapping indicates kinesin's stall force is reduced by dynein during intracellular transport. *Proc. Natl Acad. Sci. USA* **110**, 3381–3386 (2013).
28. Perur, N., Yahara, M., Kamei, T. & Tamaoki, N. A non-nucleoside triphosphate for powering kinesin–microtubule motility with photo-tunable velocity. *Chem. Commun.* **49**, 9935–9937 (2013).

Acknowledgements

The authors thank D. R. Drummond and N. Sheppard for assistance with protein purification, and T. A. McHugh for commenting on the manuscript. This research was funded by the Biotechnology and Biological Sciences Research Council (grant number BB-G530233–1) via the Systems Biology Doctoral Training Centre, University of Warwick; and the Wellcome Trust (grant number 103895/Z/14/Z).

Author contributions

D.R.P. and R.A.C. designed the experiments. N.J.B. provided mathematical insight. D.R.P. designed the analyses, collected and analysed the data, developed the microfluidics interface and produced the manuscript and figures. All the authors contributed towards the discussion and interpretation of results, and editing the manuscript.

Competing interests

The authors declare no competing interests.

Additional information

Supplementary information is available for this paper at https://doi.org/10.1038/s41565-018-0084-4.

Reprints and permissions information is available at www.nature.com/reprints.

Correspondence and requests for materials should be addressed to R.A.C.

Publisher's note: Springer Nature remains neutral with regard to jurisdictional claims in published maps and institutional affiliations.

Methods

Proteins and biochemical reagents. Tubulin was purified from pig brains as previously described[2], with additional steps as follows. Tubulin was polymerized in 50 mM PIPES, 1.2 mM $MgSO_4$, 1 mM EGTA, 1 mM GTP, 1 mM dithiothreitol (DTT) and 186 mg ml^{-1} glutamic acid, and then incubated for 60 min at 37 °C. Microtubules were centrifuged in a TLA 100.3 rotor at 85,000 revolutions per minute (r.p.m.) for 20 min at 35 °C, then resuspended in K-PEM with 1 mM GTP, 1 mM $MgSO_4$ and 1 mM DTT, cooled to 4 °C and centrifuged in a TLA 100.3 rotor at 85,000 r.p.m. for 20 min. The supernatant was run through a Hiprep 26/10 desalting column into K-PEM buffer (100 mM PIPES, 1 mM $MgSO_4$, 2 mM EGTA (Fisher), adjusted to pH 6.9 with KOH) and 20 µM GTP. Tubulin concentrations were determined using $E_{280} = 105{,}838\ M^{-1}\ cm^{-1}$.

X-rhodamine labelled tubulin was purchased from Cytoskeleton Inc. Alexa Fluor 488 (Molecular Probes)-labelled tubulin was prepared using standard protocols, as previously described[2].

Kinesin was purified as previously described[29]. Kinesin concentrations were determined using $E_{280} = 15{,}300\ M^{-1}\ cm^{-1}$.

Nucleotides were from Jena Biosciences. Other reagents were from Sigma unless stated otherwise.

Bead–mPEG (methoxypolyethylene glycol) crosslinking. Yellow-green carboxylated FluoSpheres (0.5 µm (Thermo Fisher)) were diluted to 1% solids and activated using 10 mg ml^{-1} 1-ethyl-3-(3-dimethylaminopropyl)carbodiimide in pH 6 MES buffer and mixed gently at room temperature for 30 min. Beads were then centrifuged, resuspended in 10 mg ml^{-1} of mPEG-amine 750 in pH 7.4 PBS and mixed gently at room temperature for 2 h. Adding 90 mM glycine quenched the reaction. After 30 min the beads were centrifuged and resuspended in 0.1% Tween20 in K-PEM five times and stored at 4 °C.

Flow-chamber assembly (for manual flow-through). Flow chambers were assembled from 22 × 22 mm no. 1.5 glass coverslips and 76 × 26 mm 1–1.2 mm thickness glass slides. Double-sided Scotch tape was sandwiched between the glass surfaces to form a 2 mm wide channel. The periphery of the chamber was further secured using nail polish excluding the channel ends, which were left open. Solutions were drawn through the channel by using grade 1 Whatman filter paper.

Microfluidics. Microfluidic flow chambers were assembled by stacking the following: a 50 × 22 mm no. 1.5 glass coverslip, cleaned using the protocol from the tubulin-depletion assays, or a 50 × 22 mm cyclo-olefin polymer coverslip (188 µm thick ZF14–188 (Zeon)) cut using a Silhouette Portrait plotter cutter; double-sided adhesive tape (ArCare 90445, kindly provided by Adhesives Research), with a Y-shaped channel cut using a plotter cutter (two 8 × 0.75 mm inlets that join a 22 × 1.5 mm channel) and a 40 × 22 mm COP coverslip with portholes. Chip-to-tubing connectors were assembled using ring magnets (8.16 mm outer diameter (o.d.) × 3.5 mm inner diameter (i.d.) (First4magnets)) pressed into a 3D-printed ABS magnet holder (which was later used to align the magnets with the portholes in the COP coverslip) and then cast in polydimethylsiloxane (PDMS; Sylgard 184 (Dow Corning)) to fill the ring magnets and produce a 0.8-mm-thick cushion that forms the interface between the magnets and the microfluidic chip. A 1.25 mm biopsy punch was used to bore holes through the PDMS–magnet core. Polyether ether ketone (PEEK) tubing (Upchurch) of 127 µm i.d. × 1.59 mm o.d. was inserted into the holes to form a tight seal. The flow chamber was placed on a custom ferromagnetic stainless-steel (430) microscope stage, which sealed the connections by attracting the magnets and held the sample in position. Flow was driven using an MFCS-EZ, inlets were controlled using an L-switch and the outlet flow was monitored using an M flow unit (Fluigent). A Matlab (Mathworks) function was written to integrate fully the control of the microfluidics with the microscope.

Tubulin depletion and microtubule-bending assay. Coverslips were sonicated (600 W bath (Ultrawave)) in 3% Neutracon detergent (Decon Laboratories) for 30 min at 60 °C before undergoing extensive wash–sonication cycles in ultrapure water (18.2 MΩ). A flow chamber was assembled, filled with 0.2 mg ml^{-1} poly(L-lysine)–PEG–biotin (SuSoS) and incubated for 30 min. It was washed with K-PEM before adding 1 mg ml^{-1} NeutrAvidin (Thermo Fisher Scientific) for 5 min and washing again. Microtubule seeds (polymerized using 26 µM 15% labelled Alexa488-tubulin and 1 mM GMPCPP in K-PEM at 37 °C for 25 min) were pelleted, diluted to ~ 60 nM, injected into the chamber and incubated for 5 min. After washing the chamber, dynamic microtubule extensions were grown by flowing through with 15 µM tubulin, 1 mM GTP, glucose oxidase and catalase (GOC) oxygen scavenger (4.5 mg ml^{-1} glucose, 0.2 mg ml^{-1} glucose oxidase, 35 µg ml^{-1} catalase, 0.5% (v/v) β-mercaptoethanol), 1 mg ml^{-1} bovine serum albumin (BSA) and 0.1% (v/v) Tween20 in K-PEM. Microtubules were grown for >15 min at 25 °C prior to imaging with epifluorescence and dark-field illumination. Tubulin was depleted by flowing through pre-warmed (25 °C) K-PEM, supplemented with kinesin and nucleotides as described in the main text. Microtubule bending was achieved by rapidly drawing solutions through the channel using Whatman filter paper.

Kinesin surface-clamp assay. Fluorescence controls (colour-segmented stabilized microtubules) were prepared by incubating 5 µM 30% labelled Alexa Fluor 488 tubulin and 0.2 mM GMPCPP in K-PEM at 37 °C for 60 min and pelleted in an airfuge (Beckman Coulter) at 25 psi (6.9 Pa) for 10 min. The supernatant was discarded and the pellet resuspended in pre-warmed 5 µM 30% labelled X-rhodamine tubulin and 0.2 mM GMPCPP in K-PEM. Microtubules were left to anneal at room temperature and then diluted 50-fold before use.

Coverslips were sonicated (600 W bath) at room temperature in a 1:1 solution of methanol and HCl for 30 min, and then sonicated for 5 min (four times) in ultrapure water, 60 min in 0.2 M KOH and 5 min (five times) in ultrapure water. They were spun dry using a Spin Clean (Technical video), incubated at 100 °C for 30 min and plasma cleaned (PLASMA clean 4, ILMVAC) for 5 min. Coverslips were then silanized by immersing them in 0.05% dimethyldichlorosilane in trichloroethylene for 60 min, and then washed in methanol, sonicated for 5 min (five times) in methanol and spun dry.

A flow chamber was assembled using a silanized coverslip and filled with 0.1 mg ml^{-1} anti-6x histidine antibodies (Thermo Fisher 37-2900) for 10 min. The chamber was then flushed with 0.5 mg ml^{-1} α-casein and incubated for 5 min, then with 75 nM K340 for 10 min and washed with ten chamber volumes of K-PEM. Stabilized segmented microtubules were then introduced. Unbound microtubules were washed out immediately with K-PEM. Dynamic microtubules, polymerized by incubating 50 µM 30% labelled Alexa Fluor 488 tubulin (same stock as used for the fluorescence controls) and 1 mM GTP in K-PEM for 45 min at 37 °C, were diluted 20-fold in warm (37 °C) K-PEM and immediately flowed through the chamber ahead of ten chamber volumes of warm K-PEM. The sample was imaged using epifluorescence, and ADP in K-PEM was introduced at the desired concentration. Once the microtubules had shortened sufficiently, 10 µM taxol and 200 µM ATP in K-PEM was flowed in.

Microtubule expansion assay with microfluidics. Microtubules were attached to the glass surface as in the tubulin depletion assay or by using COP coverslips, which were plasma-treated (air, 3 min), immersed in 3% (3-aminopropyl) triethoxysilane in ethanol for 2 h, placed in an ultrasonic bath in ethanol for 5 min (twice) and then washed extensively with water before drying with N_2 gas. COP flow chambers were filled with 1 mM $BS(PEG)_5$ (PEGylated bis(sulfosuccinimidyl) suberate) in PBS for 30 min, washed thoroughly with PBS, incubated with 0.1 mg ml^{-1} anti-biotin antibodies for 5 min and then 50 mM Tris buffer pH 8 for 30 min. Dynamic microtubules were polymerized following the same initial steps as for the tubulin depletion assay, except that 20 µM 10% X-rhodamine-labelled tubulin was used to grow dynamic extensions, which were left for 1 h to polymerize. Buffer exchanges were performed using the microfluidic pump. Microtubules were capped by incubating with 6 µM 15% Alexa-488 tubulin + 1 mM GMPCPP for 20 min before switching to 1% Tween20 for 5 min. Two pressure lines were calibrated to achieve the same user-defined flow rate immediately before imaging with TIRF microscopy. K-PEM with 1 × GOC, 1% Tween20, 0.02% methylcellulose (1,500 cP) and 1 mg ml^{-1} casein or 2 mg ml^{-1} BSA was flowed through with either 1 mM ADP + 0.003–0.01% mPEG-beads or 200 nM K340, alternating every 2 s frames (80 times), cycling three times. The images shown are background-subtracted in the green imaging channel by subtracting the median and applying a rolling ball ($r = 200$) to each frame using Fiji.

Surface-stitched microtubule expansion assay. Coverslips were incubated in 1 M HCl at 50 °C for 12–15 h, rinsed with ultrapure water twice, sonicated in ultrapure water for 30 min, sonicated in ethanol for 30 min, rinsed in ethanol and dried by spinning or using nitrogen gas. Microtubules were polymerized as in the microtubule expansion assay with microfluidics, except that the microtubule seeds and caps were labelled to 30% with Alexa488 and dynamic extensions were grown using unlabelled tubulin. Microtubules were capped for 10 min before washing with 100 µl of 0.1% Tween in K-PEM. Hereafter, each buffer contained GOC, 0.1% Tween20 and 0.02% methylcellulose (4,000 cP) in K-PEM. The chamber was washed with 30 µl of buffer before imaging. During imaging, 40 µl of 200 nM K340 was flowed through by hand, followed later by 40 µl of 1 mM ADP. Flowing through 100 µl of buffer depleted the ADP, after which a new field of view could be imaged and the kinesin and ADP flows repeated. We imaged no more than five times in a single flow chamber.

Dark-field/epifluorescence microscopy. Images were captured by an electron-multiplying charge-coupled device (EMCCD) camera (iXon^{EM} + DU-897E, Andor) fitted to a Nikon E800 microscope with a Plan Fluor 100 × NA 0.5–1.3 (NA, numerical aperture) variable iris objective. A custom-built enclosure with an air heater (Air-Therm ATX, World Precision Instruments) was used to keep samples at 25 °C. Dark-field illumination was achieved using a 100 W mercury lamp connected to the microscope via a fibre optic light scrambler (Technical video), cold mirror, 500–568 nm band-pass filter (Nikon) and a dark-field condenser (Nikon). A stabilized mercury lamp (X-Cite exacte, Lumen Dynamics) provided illumination for epifluorescence, connected to the microscope with a light pipe. Motorized filter wheels (Ludl Electronic Products) housed the fluorescence excitation and emission filters: 485/20 and 536/40 for Alexa-488 and 586/20 and 628/32 for X-rhodamine (Chroma). Combined dark-field and fluorescence

imaging was achieved using an FF505/606-Di01–25×36 dichroic mirror (Semrock) and electronic shutters to switch between the illumination modes. The shutters, filter wheels and camera were controlled using Metamorph software (Molecular Devices).

TIRF microscopy. Images were captured by an EMCCD camera (iXon$_3$ 888, Andor) fitted to a Warwick Open-Source Microscope (WOSM), which was equipped with 473 nm (Cobolt) and 561 nm (Obis) laser lines, a Di01-R488/561 dichroic mirror (Semrock), a Nikon 100×NA 1.49 TIRF objective and ZET473NF and ZET561NF emission filters (Chroma). Acquisition was triggered using a Matlab script, which used Micromanager to capture images, launched WOSM macros for all other microscope functionality and controlled and monitored the microfluidics. Pixels were 130 nm. Data were acquired at 23 °C.

Analysis of microtubule shrinkage rates. Data were analysed in Matlab (Mathworks). Kymographs were generated by averaging the cross-section of a straight-line ROI over 11 pixels (rotated by using the imrotate function first) for each frame of an image stack. Shrinkage rates were measured by manually tracing kymographs using the impoly function and calculating the slope. Time and distance calibration was automated using the image metadata. The rates in this paper assume a conversion of 125 dimer $PF^{-1} = 1\,\mu M$. A fluorescence analysis of kinesin surface-clamp data is presented in Supplementary Methods. Plotting and statistical tests were also carried out using Matlab.

Analysis of microtubule expansion assay with microfluidics. Microtubules were carefully selected for analysis, rejecting any that did not conform to their original trajectory at the end of an ADP–kinesin cycle, which was assessed by visual inspection. Kymographs were generated using the Fiji plugin KymoResliceWide with a 15 pixel cross-section. Subsequent analysis was performed using Matlab. Expansion of the microtubule was measured for each time point, as shown in Supplementary Fig. 5. These measurements were then analysed for each ADP or kinesin interval: the mean expansion value was taken for each ADP interval, whereas a logistic curve was fitted (using bisquare robust fitting) to each ADP-kinesin transition to estimate the kinesin-driven expansion (as shown in Fig. 5d).

Analysis of surface-stitched microtubule expansion assay. The coordinates of the microtubules were extracted from dark-field images using the Fiji plugin JFilament[30], mapped onto the fluorescence channel and used to generate a linescan 5 pixels wide. Fluorescence profiles of the cap and seed were each fitted with a Gaussian error function in Matlab. The length of the GDP-microtubule is given by the distance between the point of inflection on each curve. The microtubule length change was then assessed by taking the mean length of the manually identified plateaus, as shown in Supplementary Fig. 4b. Points that deviated by more than 5% from the median in these intervals were discarded before fitting. The average length of the kinesin-free GDP microtubules analysed for this paper was 41 µm.

Data availability. The data that support the plots within this paper and other findings of this study are available from the corresponding author on reasonable request.

References

29. Crevel, I. et al. What kinesin does at roadblocks: the coordination mechanism for molecular walking. *EMBO J.* **23**, 23–32 (2004).
30. Smith, M. B. et al. Segmentation and tracking of cytoskeletal filaments using open active contours. *Cytoskeleton* **67**, 693–705 (2010).